European Journal of Medicinal Chemistry 238 (2022) 114449

Contents lists available at ScienceDirect

European Journal of Medicinal Chemistry

journal homepage: www.elsevier.com/locate/ejmech

Study of the anticancer potential of Cd complexes of selenazoyl-hydrazones and their sulfur isosters

Sanja B. Marković [a], Natalia Maciejewska [b], Mateusz Olszewski [b], Aleksandar Višnjevac [c], Adrián Puerta [d], José M. Padrón [d], Irena Novaković [e], Snežana Kojić [f], Henrique S. Fernandes [g], Sérgio F. Sousa [g], Sandra Ramotowska [h], Agnieszka Chylewska [h], Mariusz Makowski [h], Tamara R. Todorović [a], Nenad R. Filipović [i,*]

[a] University of Belgrade - Faculty of Chemistry, Studentski Trg 12-16, 11000, Belgrade, Serbia
[b] Department of Pharmaceutical Technology and Biochemistry, Faculty of Chemistry, Gdansk University Technology, Narutowicza 11/12, 80-233, Gdansk, Poland
[c] Division of Physical Chemistry, Institute Ruđer Bošković, Bijenička Cesta 54, 10000, Zagreb, Croatia
[d] BioLab, Instituto Universitario de Bio-Orgánica "Antonio González", Universidad de La Laguna, 38206, La Laguna, Spain
[e] Institute of Chemistry, Technology and Metallurgy, University of Belgrade, Njegoševa 12, 11000, Belgrade, Serbia
[f] Laboratory for Molecular Biology, The Institute of Molecular Genetics and Genetic Engineering, University of Belgrade, Vojvode Stepe 444a, 11000, Belgrade, Serbia
[g] UCIBIO@REQUIMTE, BioSIM, Departamento de Biomedicina, Faculdade de Medicina, Universidade Do Porto, Porto, Portugal
[h] Faculty of Chemistry, University of Gdansk, Wita Stwosza 63, Gdansk, PL80-308, Poland
[i] University of Belgrade - Faculty of Agriculture, Nemanjina 6, 11000, Belgrade, Serbia

ARTICLE INFO

Keywords:
Hydrazonyl-thiazoles
Cd complexes
DNA interactions
Apoptosis
Autophagy

ABSTRACT

The biological activity of Cd compounds has been investigated scarce since Cd has been recognized as a human carcinogen. However, the toxicity of cadmium is comparable to the toxicity of noble metals such as Pt and Pd. The paradigm of metal toxicity has been challenged suggesting that metal toxicity is not a constant property, yet it depends on many factors like the presence of appropriate ligands. Studies on anticancer activity of cadmium complexes showed that the complexation of various ligands resulted in complexes that showed better activities than approved drugs. In the present study, cadmium complexes with biologically potent thiazolyl/selenazoyl-hydrazone ligands have been prepared, and tested for their activity against different types of tumor cell models. The complexation of ligands with Cd(II) resulted in a synergistic effect. The antiproliferative activity study revealed that all complexes are more active compared to 5-fluorouracil and cisplatin. The mechanism of tumor cell growth inhibition reveal that selenium-based compounds induce cell death in T-47D (gland carcinoma) cells through apoptosis *via* caspase-3/7 activation. Additionally, their pro-apoptotic effect was stronger compared to etoposide and cisplatin. Nuclease activity, detected by gel electrophoresis, may be the possible mechanism of anticancer action of investigated complexes.

1. Introduction

Nowadays, medicinal chemistry is mainly focused on organic compounds, which represent more than 99% of approved drugs [1]. Despite the fact that metal-based compounds (MBCs) are used for the treatment of various diseases since the beginning of modern medicine [2], they are much less investigated as potential drugs. There are multiple reasons for that, such as metal toxicity, low solubility, multi-targeting properties as well as high molecular weight (MW > 500 Da) which is not in accordance with Lipinski's rule of 5 which defines oral bioavailability of potential drugs. On the other hand, MBCs show unique mechanisms of action, which are not accessible to organic compounds themselves [3]. Additionally, MBCs cover different chemical space in comparison to organic compounds, which are characterized by higher 3D character. The higher 3D character of compounds is recognized as an important factor that enhances the possibility of their clinical application [4]. Nowadays, there is a paradigm shift regarding the treatment of multifactorial diseases from single-targeting to multi-targeting agents [5]. Therefore, MBCs are recognized as promising scaffolds for the treatment of diseases like cancer [6]. The development of novel delivery systems

* Corresponding author.
E-mail address: nenadf@agrif.bg.ac.rs (N.R. Filipović).

https://doi.org/10.1016/j.ejmech.2022.114449
Received 18 August 2021; Received in revised form 5 May 2022; Accepted 6 May 2022
Available online 12 May 2022

appears to be a promising strategy to overcome low solubility and low bioavailability, as well as the high toxicity of MBCs [7].

The usage of MBCs in the modern era of medicinal chemistry started with the approval of *cis*-diamminedichloroplatinum (II) (cisplatin or CDDP) for cancer treatment more than 50 years ago (Table S1 is shown in Electronic Supplementary Information, ESI). The main target of this platinum-based drug, as well as its six structural analogues approved for cancer treatment, is DNA. All approved platinum-based drugs, called platins, bind covalently to DNA bases, cause mostly intra-strand cross-links, and consequently induce apoptosis of cancer cells [8]. Cisplatin, oxaliplatin, and carboplatin are applied in almost 50% of second therapy regimes and are included in the "list of essential medicines" published by the World Health Organization [2]. The great success of platins in cancer treatment triggered an investigation of the anticancer properties of non-platinum metal compounds. Because of such efforts, three novels MBCs based on Al, Pd, and Lu, for which photoactivation was determined as the mechanism of action, have been approved for cancer treatment (Table S1, ESI). In addition, MBCs based on other metals, whose activity relies on various mechanism of action, reached clinical trials for cancer treatment worldwide.

The biological activity of Cd compounds has been investigated scarce since Cd has been recognized as a human carcinogen by the International Agency for Research on Cancer (IARC) [9]. Nevertheless, data are indicating that the toxicity of cadmium is comparable to the toxicity of noble metals such as Pt and Pd [10]. Also, the paradigm of metal toxicity has been challenged recently. Egorova & Ananikov [11] suggested that metal toxicity is not a constant property, yet it depends on many factors. Some results indicate that cadmium, when complexed with appropriate ligands, can show favorable anticancer activity [12]. Studies on anticancer activity of cadmium complexes showed that the complexation of various ligands resulted in complexes that showed better activities than corresponding ligands, complexes with metals different from cadmium, and approved drugs [13]. Mechanistic studies showed that Cd complexes target not only DNA, but also several protein targets such as proteasomal chymotrypsin-like, proteasomal deubiquitinase, histone deacetylase, and telomerase [13]. Cd complexes also inhibit the incorporation of 3H-thymidine into DNA and the respiration of tumor cells and kill cancer cells *via* programmed cell death apoptosis [13].

(1,3-Thiazolyl-2-yl)hydrazones (THs) are thiazole derivatives known for their various biological activities, including antimicrobial and anticancer activity, as well as their antioxidant capacity [14]. In our previous work, we investigated the biological activity of a focused library of three pyridine-based THs (Fig. 1), as well as their selenium analogues (1,

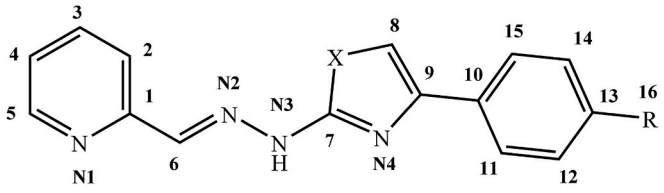

Ligands			Complexes	
Label	R	X	Label	Bruto formula
HLS^1	H	S	**1-S**	$[Cd(HLS^1)_2](ClO_4)_2$
HLS^2	OMe		**2-S**	$[Cd(HLS^2)_2](NO_3)_2 \cdot H_2O$
HLS^3	Me		**3-S**	$[Cd(HLS^3)_2](ClO_4)_2 \cdot H_2O$
HLSe^1	H	Se	**1-Se**	$[Cd(HLSe^1)_2](ClO_4)_2$
HLSe^2	OMe		**2-Se**	$[Cd(HLSe^2)_2](NO_3)_2 \cdot MeOH$
HLSe^3	Me		**3-Se**	$[Cd(HLSe^3)_2](ClO_4)_2$

Fig. 1. Labeling of the ligands and complexes used in this study.

3-selenazolyl-2-yl)hydrazones (SHs) [14]. Antiproliferative activity study conducted on six human solid tumor cell lines showed that the potency of THs and SHs against non-small cell lung carcinomas A549 and SW1573 and spontaneously immortalized breast cell line HBL-100 cells was comparable to 5-fluorouracil (5-FU), in most cases, while none of the compounds was active against colon adenocarcinoma cell line WiDr. Activity against gland carcinoma (T-47D) in the low micromolar range was observed for **HLSe^1** and **HLSe^2**, while **HLS^2**, **HLSe^3**, and **HLS^3** were not active.

In the present paper, we report the synthesis of the Cd complexes with **HLS$^{1-3}$** and **HLSe$^{1-3}$** ligands and study of the impact of chalcogen atom type and substitution on the ligands' periphery on anticancer activity.

2. Results and discussion

2.1. Chemistry

In order to prepare Cd complexes with **HLS$^{1-3}$** and **HLSe$^{1-3}$** ligands, methanol solution of the appropriate ligand and $Cd(ClO_4)_2 \cdot 6H_2O$ in the molar ratio 2 : 1 was heated under reflux for 1 h. The single crystals of complexes **1–S**, **3–S**, **1–Se**, and **3–Se**, suitable for X-ray diffraction analysis, were obtained after few days from the mother liquor. However, the complexes **2−S** and **2−Se** were obtained in the form of microcrystals, and recrystallization did not give quality single crystals. Because of that, we used an anion replacement strategy. Single crystals of **2−S** and **2−Se** were obtained after few days from mother liquor when $Cd(NO_3)_2 \cdot 4H_2O$ was used instead of $Cd(ClO_4)_2 \cdot 6H_2O$. All the complexes are 2 : 1 type of electrolytes, while results elemental analysis are consistent with the formulas given in Fig. 1. The IR, ^1H, and ^{13}C NMR spectra of the ligands and complexes are shown in ESI (Fig. S1−S42).

Reported structures present six homoleptic distorted octahedral cadmium complexes, where tridentate ligands are coordinated *via* three nitrogen donor atoms emanating from thiazole/selenazole, azomethine, and pyridine moieties. ORTEP molecular structures of the complexes are given in Fig. 2. Basic crystallographic data are given in Table S2 (ESI). All six complexes crystallize in a monoclinic crystal system but in different space groups *C*2/*c* (**1–S**, **1–Se**), $P2_1/n$ (**2–S**, **3–S**, **2–Se**), and *I*2/*a* (**3–Se**) (Table S2, ESI). Geometric parameters of the coordination spheres are given in Tables S3 and S4 (ESI). The coordination spheres in all six complexes are very similar. Their severe distortion from the parameters characteristic of an ideal octahedron is caused by the small bite angles (bold values in Table S4, ESI) imposed by the geometries of tridentate ligands. The geometric features of an octahedron are, to a certain extent, retained only by coordination valence angles involving pairs of analogous nitrogen donor atoms from the two coordinating ligand molecules. The bite angles reported hereby are in accordance with the mean value of the bite angles [$\alpha_{mean} = 72\ (3)^\circ$] revealed by a set of 73 structures of cadmium complexes extracted from the current version of the Cambridge Structural Database (CSD) [15]. Only the extracted structures with the final *R* factor lower than 0.075 and with five-membered coordination rings involving neighboring donor atoms were considered. Valence angles N2–Cd–N6 (involving two azomethine nitrogen donors) approach 180° while valence angles N4–Cd–N8 and N1–Cd–N5, involving pairs of thiazole/selenazole and pyridine nitrogen donor atoms, respectively, are fairly close to 90°. All other valence angles reveal severe distortion of the coordination spheres. In the structures **1–S**, **1–Se,** and **3–Se**, the central Cd(II) ion lies on the 2-fold crystallographic axis, with a half of the each complex molecule in the asymmetric unit. Crystal packing of all complexes is based on classical hydrogen interactions. Description and parameters of interactions are shown in ESI (Table S5, Fig. S43).

All studied ligands exhibit chelating properties towards cadmium ions that is reflected in spectral changes during performed titrations: (i) a reduction of the intensity of the ligand absorption maxima at ca 260 and 350 nm and (ii) formation of a new intense absorption maximum at

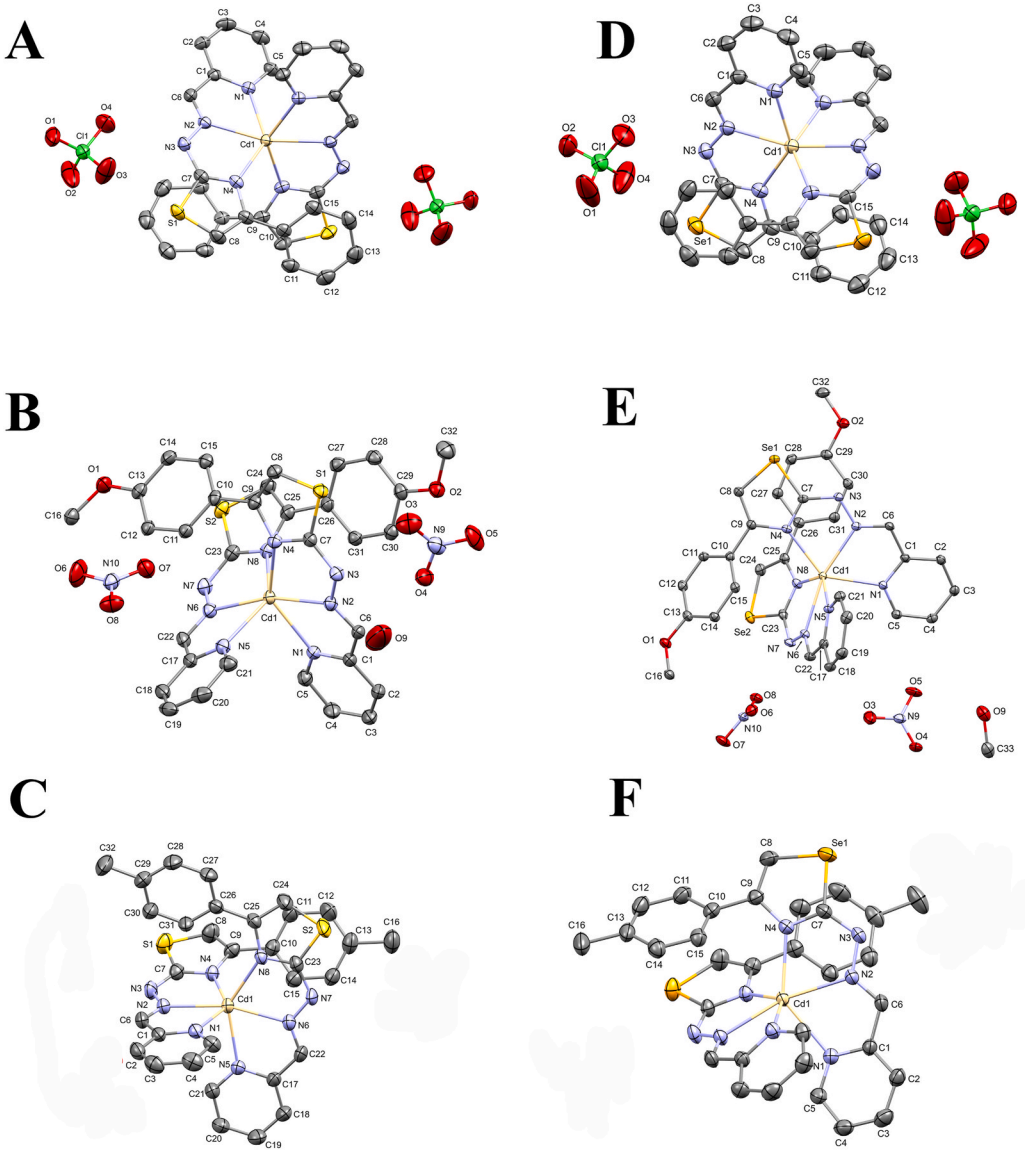

Fig. 2. ORTEP drawings of molecular structures of **1–S** (A), **2–S** (B), **3–S** (C), **1–Se** (D), **2–Se (E)**, and **3–Se** (F). Thermal ellipsoids are given at the 30% probability level. Hydrogen atoms are omitted for clarity. Disordered perchlorate anions (**3–S** and **3–Se**) and water molecules (**3–S**) are removed for clarity.

ca 450 nm. For **HLS**$^{1-3}$ ligands (Figs. S44–S46, ESI), an increase in the intensity of the ligand band at ca. 205 nm was observed, while for **HLSe**$^{1-3}$ the opposite trend was observed (Figs. S47–S49, ESI). In the case of **HLSe**$^{1-3}$ titrations, the shape of the UV–Vis spectra is similar to HLS$^{1-3}$, but the changes in the intensity of absorption maxima are more subtle.

The performed titrations allowed determining the dependence of the changes in absorbance on the molar metal: ligand ratio. This enabled the assessment of obtained complex ions stoichiometry and the calculation of stability constant values. For all studied derivatives, in the absorbance *vs* c_M/c_L graphs, the curve inflection was observed at the ratio of 0.5. This indicates the formation of $[M(HL)_2]^{2+}$ complex ions. Therefore, for all $[M(HL)_2]^{2+}$ complexes, the values of the cumulative stability constant β_{12} were calculated (Table 1). Since the ligands coordinate sequentially to the metal ion, the 1 : 1 stoichiometry forms of $[M(HL)]^{2+}$ complex cations are certainly also present in the solutions. Hence, the gradual constant K_{11} values, describing this equilibrium were also calculated. Based on the dependencies between the gradual and cumulative stability constants, the values of the K_{12} constants, describing the equilibrium of attachment the second ligand to the $[M(HL)]^{2+}$ complex cations, were also determined and presented in Table 1.

Table 1
Values of gradual and cumulative stability constants of studied ligands complexes with cadmium ions.

Complex	log K_{11}	log K_{12}	log β_{12}
1–S	5.27 ± 0.27	3.99	9.26 ± 0.21
2–S	6.11 ± 0.32	3.06	9.17 ± 0.59
3–S	6.09 ± 0.43	3.86	9.95 ± 0.38
1–Se	5.93 ± 0.22	3.90	9.83 ± 0.66
2–Se	6.19 ± 0.35	4.70	10.89 ± 0.47
3–Se	5.89 ± 0.29	4.54	10.43 ± 0.52

Obtained values of cumulative stability constant β_{12} indicate the significant stability of **1–3S** and **1–3Se** chelate complexes. Despite smaller changes in the UV–Vis spectra during titrations, **1–3Se** are characterized by greater stability of the $[M(HL)_2]^{2+}$ complexes formed in the solution, as evidenced by higher values of logβ. Among this group of compounds, the derivative with a methoxy substituent (**HLSe**^{2}) has the highest value of the cumulative stability constant, which proves the highest stability of the **2-Se** complex in solution. In the case of sulfur

derivatives, the complex with a methyl-substituted ligand (**HLS^3**) has the highest value of the β_{12} constant.

2.2. Biological assessment

2.2.1. Antiproliferative activity

The antiproliferative activity of **1–3S** and **1–3Se** was evaluated *in vitro* against six human cell lines: non-small cell lung carcinomas A549 and SW1573, cervical adenocarcinoma HeLa, spontaneously immortalized breast cell line HBL-100, colon adenocarcinoma WiDr, and gland carcinoma T-47D, using Sulforhodamine B (SRB) colorimetric assay. A non-tumor HEK293 cell line (human embryonic kidney) was also used for analyzing the selectivity. The half-maximal growth inhibitory concentration (GI_{50}) values were calculated for each compound. For comparison, obtained results together with results previously published for **HLS$^{1–3}$** and **HLSe$^{1–3}$** [16] are presented in Table 2, while Fig. 3 depicts GI_{50} ranges against human solid tumor cell lines for all investigated compounds. Since all ligands were inactive against WiDr cell line (i.e. $GI_{50} > 100$ μM), the plot does not include GI_{50} values of the ligands on this cell line. All six complexes showed better anticancer activities compared to selenium- and sulfur-based ligands. Each tested compound showed remarkable anticancer activity against almost all tested cell lines, indicating congruous GI_{50} values around 2 μM. Our previous studies showed that selenium- and sulfur-based compounds inhibited cell proliferation in human lung, breast, colon, and cervical cells in micromolar concentrations [14]. The ligands within two groups differ only in the nature of the R substituent. However, this small structural difference has a great impact on their antiproliferative activity. As already discussed in our previous publication [14], sulfur-based ligands, which are generally less active, have higher values of calculated polar surface area (PSA). Due to the highest PSA value among all ligands, **HLS^2** is the most polar and inactive against all tested human tumor cell lines (Table 2), probably due to incompatibility between its polar surface and hydrophobic surface of active sites of potential biological targets [14]. Among SH ligands, **HLSe^1** and **HLSe^2** possess the most pronounced cytotoxic activity, **HLSe^2** being the two times more active on SW1573 and HBL-100 cell lines than **HLSe^1**. The difference in the activity can be related to the difference in drug-likeness parameters and local reactivity properties, as previously discussed [14].

Complexation of selenium-based compounds revealed approximately two-fold greater antiproliferative potency than metal-free ligands in A549, HBL-100, HeLa, SW1573 cells. None of the selenium-ligands showed activity against WiDr cells, which have low sensitivity to 5-FU ($GI_{50} = 49.0 \pm 6.7$ μM), unlike their Cd(II) complexes. In the T-47D cell line, which is extremely resistant to estrogens and antiestrogens, **1–Se** and **2–Se** complexes showed four-fold and three-fold lower GI_{50}, respectively, in comparison to the ligands alone [17]. Complex **3–Se** is a highly active compound ($GI_{50} = 1.9 \pm 0.3$ μM), while the ligand core showed no antiproliferative activity on the T-47D cell line.

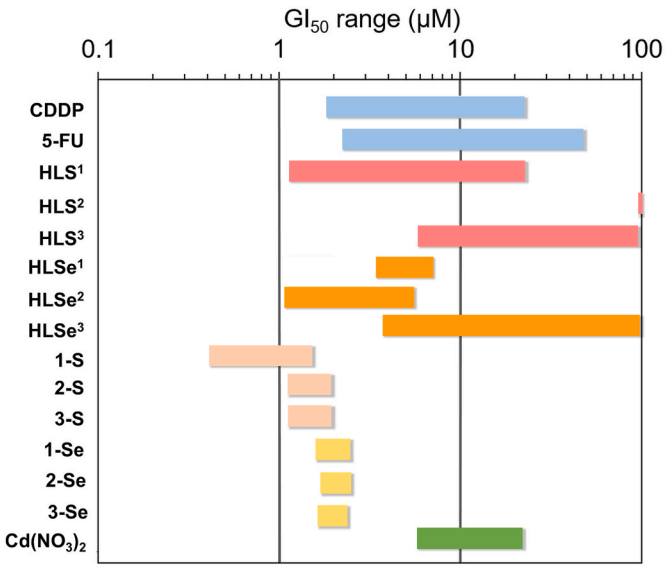

Fig. 3. GI_{50} range plot against human solid tumor cell lines of investigated ligands, corresponding Cd(II) complexes, reference drugs and Cd-salt.

Sulfur-based ligands exhibited generally inferior anticancer potency in comparison to selenium-based ligands. Interestingly, the antiproliferative capacity of the sulfur-based ligands was significantly improved upon complexation to cadmium ions. Indeed, **1–S** showed similar GI_{50} values as its corresponding ligand **HLS^1** on most of the tested cell lines, except on T-47D and WiDr cells, where GI_{50} values for the complex were significantly lower. The Cd(II) complex **2–S** showed GI_{50} values below 2 μM on all tested cell lines, while its ligand (**HLS^2**) was generally inactive in SRB assay. Similarly, the complexation of the ligand **HLS^3** notably improved the anticancer activity of the compound, except on SW1573 cell line, where GI_{50} was only two-fold lower after complexation. Noteworthy, the GI_{50} values obtained for our new compounds (0.7–2.5 μM) in most cases were much lower than those of 5-FU (2.2–49 μM) or those of cisplatin (1.9–26.6 μM). Also, significantly higher GI_{50} values obtained for $Cd(NO_3)_2$, when compared to the

Table 2
The antiproliferative activities (GI_{50}) on six human tumor cell lines and healthy cell line and LC_{50} values of the *A. salina* cytotoxic activity test for **1–3S, 1–3Se** and ligands **HLS$^{1–3}$** and **HLSe$^{1–3}$**.

GI_{50} (μM)								LC_{50} (μM)
Label	A549	SW1573	HBL-100	HeLa	T-47D	WiDr	HEK293	
HLS^1	3.0 ± 1.1	1.2 ± 0.2	5.8 ± 1.7	5.2 ± 1.1	22 ± 0.9	n.a.[a]	3.7 ± 1.3	60.64 ± 9.23
1-S	1.1 ± 0.2	0.7 ± 0.2	1.1 ± 0.2	0.4 ± 0.1	1.4 ± 0.3	1.3 ± 0.5	1.0 ± 0.4	85.14 ± 10.29
HLSe^1	2.9 ± 0.4	2.4 ± 0.7	4.0 ± 0.7	3.6 ± 0.7	7.2 ± 0.2	n.a.	30 ± 4	94.73 ± 6.56
1-Se	2.5 ± 0.7	1.8 ± 0.4	1.6 ± 0.1	1.7 ± 0.3	1.9 ± 0.2	2.4 ± 0.4	8.9 ± 0.1	60.72 ± 9.13
HLS^2	n.a.	n.a.	n.a.	n.a.	n.a.	n.a.	26.0 ± 0.7	144.99 ± 11.23
2-S	1.3 ± 0.1	1.1 ± 0.1	1.3 ± 0.3	1.2 ± 0.3	1.4 ± 0.4	1.9 ± 0.2	2.5 ± 0.3	93.48 ± 15.88
HLSe^2	2.1 ± 0.3	1.1 ± 0.1	2.1 ± 0.6	2.8 ± 0.3	5.4 ± 0.2	n.a.	22.0 ± 4.2	137.15 ± 13.10
2-Se	1.7 ± 0.3	2.5 ± 0.2	1.7 ± 0.1	1.7 ± 0.2	1.7 ± 0.1	2.0 ± 0.2	12 ± 1	70.44 ± 10.36
HLS^3	41 ± 18	4.7 ± 0.4	n.a.	42 ± 11	n.a.	n.a.	79 ± 19	70.62 ± 7.04
3-S	1.3 ± 0.04	1.10 ± 0.08	1.5 ± 0.3	1.1 ± 0.2	1.7 ± 0.3	1.9 ± 0.6	3.0 ± 0.4	97.76 ± 21.06
HLSe^3	4.6 ± 1.3	2.6 ± 0.5	5.5 ± 0.8	3.8 ± 0.3	n.a.	n.a.	n.a.	120.14 ± 12.45
3-Se	2.0 ± 0.2	2.2 ± 0.1	2.2 ± 0.5	1.6 ± 0.1	1.9 ± 0.3	2.4 ± 0.1	14.0 ± 1.6	79.05 ± 15.96
$Cd(NO_3)_2$	19.0 ± 1.7	20.0 ± 4.6	15.0 ± 1.1	5.8 ± 1.1	22.0 ± 0.6	20 ± 1	6.2 ± 0.2	602.11 ± 13.37
5-FU	2.2 ± 0.3	3.3 ± 1.2	4.4 ± 0.7	16.0 ± 4.5	43 ± 16	49.0 ± 6.7	6.2 ± 1.8	n.d.[b]
cisplatin	4.9 ± 0.2	2.7 ± 0.4	1.9 ± 0.2	1.8 ± 0.5	17.0 ± 3.3	23.0 ± 4.3	8.2 ± 0.3	269 ± 21

[a] n. a. = not active, i.e. $GI_{50} > 100$ μM.
[b] n. d = not determined.

complexes and the ligands, indicate that the antiproliferative potential of the complexes is a result of synergistic action between Cd(II) ions and corresponding ligands.

Regarding activity on the non-cancerous HEK293 cell line, sulfur-based ligands showed higher toxicity than their selenium counterparts did. This observation is in accord with the previous data obtained from a comparative toxicity study of selenosemicarbazones and thiosemicarbazones, the precursors of SHs and THs, conducted by Agrawal et al. [18]. Complexation with Cd resulted in species that are more toxic. GI_{50} values for the complexes are in the low micromolar range, but comparable to the GI_{50} values of 5-FU and cisplatin. The application of drug delivery systems developed for cationic metal complexes, such as

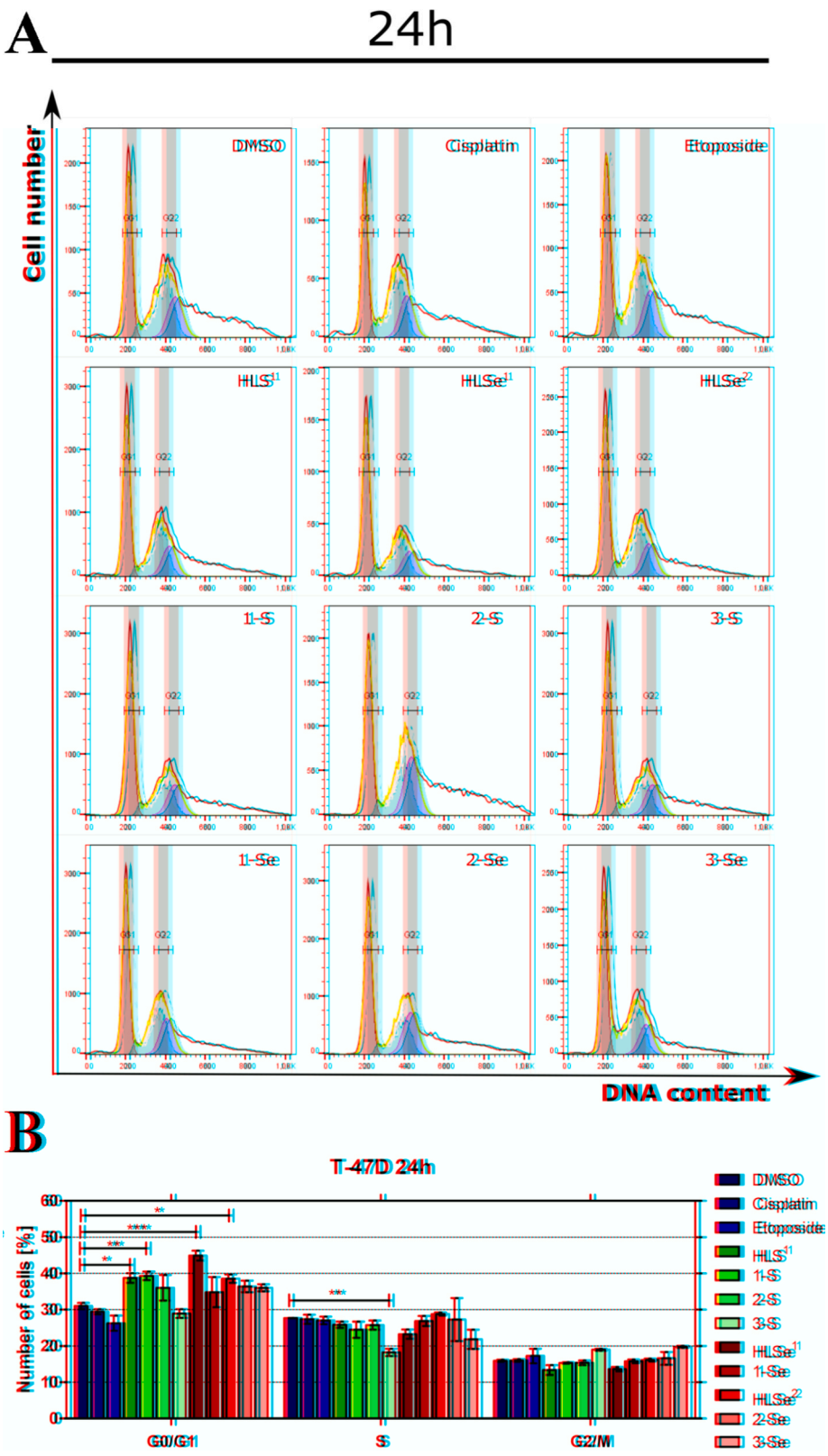

Fig. 4. Effect of tested compounds on the cell cycle of T-47D cells after 24 h of treatment. DMSO, etoposide, and cisplatin were used as reference compounds. (A) Representative histograms after PI staining measured by flow cytometry (B) The quantitation of analysis presented on a graph bar. Error bars represent the SEM of data obtained in n = 3 independent experiments. Statistical differences were analyzed with a two-way ANOVA test. ns > 0.05, *p < 0.01, **p < 0.001, ***p < 0.0001 compared to DMSO.

inorganic nanoparticles, MOFs, amphiphilic copolymers-based micelles and liposomes, etc. [7] capable to deliver metal complexes directly to tumor sites may address this drawback.

2.2.2. Acute toxicity

As a preliminary toxicity screening, *in vivo* acute lethality of **1–3S, 1–3Se**, and reference compound cisplatin was tested on brine shrimp *A. salina* after 24 h incubation. Obtained results, expressed as LC_{50} values, are presented in Table 2, together with the previously published results for **HLS$^{1–3}$** and **HLSe$^{1–3}$** [19]. Dimethyl sulfoxide (DMSO), as a negative control, did not cause changes in the viability of treated nauplii. Obtained results indicate that complexes are more toxic than corresponding ligands, while **1–3Se** are more toxic than **1–3S**. There is the same trend of toxicity within both series: **1S(e)** > **2S(e)** > **3S(e)**. Although investigated compounds are more toxic than cisplatin, obtained LC_{50} values are up to 212-fold higher (for **1-S**) in comparison to GI_{50} values from cancer cytotoxicity (Table S7, ESI). Many studies report a strong correlation between the brine shrimp lethality assay and

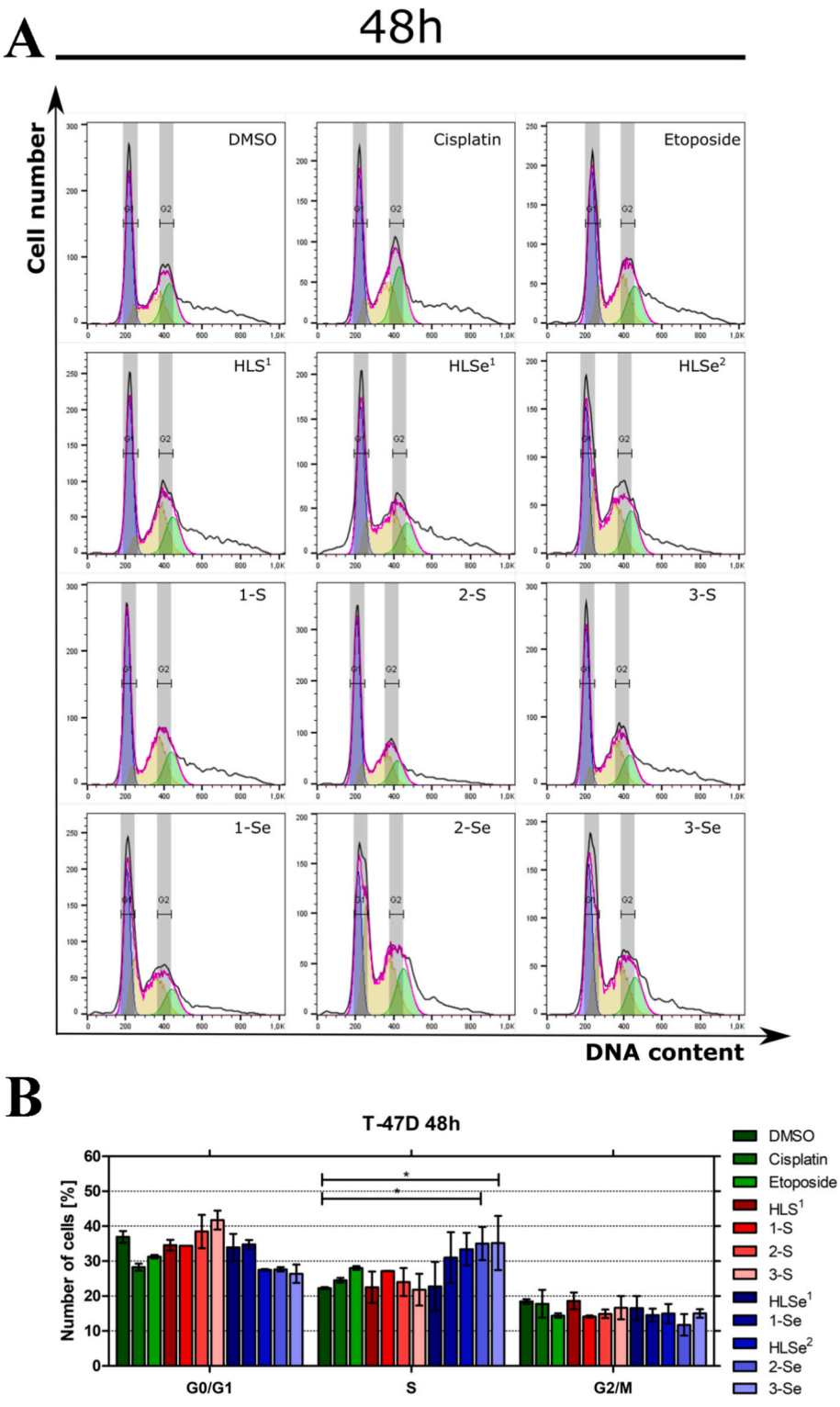

Fig. 5. Effect of tested compounds on the cell cycle of T-47D cells after 48 h of treatment. DMSO, etoposide, and cisplatin were used as reference compounds. (A) Representative histograms after PI staining measured by flow cytometry (B) The quantitation of analysis presented on a graph bar. Error bars represent the SEM of data obtained in n = 3 independent experiments. Statistical differences were analyzed with a two-way ANOVA test. ns > 0.05, *p < 0.01, **p < 0.001, ***p < 0.0001 compared to DMSO.

cytotoxicity assays and *in vivo* acute oral toxicity assay in mice [16,20,21]. Thus, we conclude that our compounds do not exhibit significant toxic effects.

2.2.3. Changes in the distribution of cell cycle phases and DNA content

Due to the high cytotoxic activity against the T-47D breast cell line and its frequent resistance to conventional anticancer therapy, further experiments were conducted on this cell line to elucidate the molecular mechanism of these compounds [22]. Compounds **HLS^2**, **HLS^3**, and **HLSe^3** do not exhibit anticancer activity, so they were not further assessed in biological evaluation. To examine whether the high cytotoxic activity of the investigated compounds (**HLS^1**, **1–3S**, **HLSe$^{1-2}$**, **1–3Se**) was caused by the cell cycle arrest, DNA content was analyzed by flow cytometry (Figs. 4 and 5). After 24 h of treatment with GI_{50} of all compounds, we generally observed slight changes in the proportion of cells in the G0/G1 phase. Ligands **HLS^1**, **HLSe^1**, and **HLSe^2** significantly increased the number of cells in this phase (p-value < 0.05) unlike its counterparts after complexation, except **1–S**, which elevated G0/G1 phase cell to 39.4%. However, observed G0/G1 arrest was only temporary, as evidenced by parallel to the vehicle distribution of cell cycle phases after 48 h of exposure. Treatment with **3-S** decreased the percentage of cells in the S phase from 27.7% (control) to 18.3%, but this effect was observed merely after 24 h of the treatment. Interestingly, the reference compounds, 5-FU, and cisplatin did not cause significant changes in the cell cycle of the T-47D cell line. Compared with the control, 48 h of treatment with **2–Se** and **3–Se** led to the arrest cell cycle at the S phase, and the accumulation of cells in this phase was elevated about 1.5-fold and 1.4-fold with **2–Se** and **3–Se**, respectively. This increase was coupled with a decreased percentage of cells in the G0/G1 phase. Because DNA replication occurs during the S-phase, we assumed that **2–Se** and **3–Se** S-phase arrest could be the result of the abrogation of DNA replication.

2.2.4. Compounds effectively inhibit the growth of breast cancer cells through the induction of apoptosis

Apoptosis, autophagy, and necrosis are the dominant types of cellular death [23]. Among these three major cell death pathways, most of the small-molecule anticancer drugs employ their cytotoxic effect *via* apoptosis, which is monitored by the Annexin-V-FITC/PI dual staining method. Annexin V-FITC is a fluorescent probe exhibiting a high affinity for phosphatidylserine, which is translocated to the outer leaflet of the cellular membrane in the initial step of apoptosis [24]. While PI allows to detection of late apoptotic and necrotic cells with disrupted integrity of the plasma and nuclear membranes by its capacity to pass through the membranes and intercalate to nucleic acids [25]. The populations of Annexin V-FITC negative/PI negative cells (live), Annexin V-FITC positive/PI negative cells (early apoptosis), Annexin V-FITC positive/PI positive cells (late apoptosis), and Annexin V-FITC negative/PI positive cells (necrotic) were evaluated by flow cytometry. Representative dot-plots and quantitative analyses are presented in Figs. 6 and 7.

After 24 h of treatment T-47D cells with sulfur-based compounds at its GI_{50} concentration, apoptotic and necrotic cells were barely detected. More prolonged exposure to sulfur-based compounds (48 h) increased the Annexin V-FITC (+)/PI (+) cells fraction, from 10.9 ± 1.4% (control) to 20.3 ± 0.8% and 22.1 ± 1.9% for **2–S**, and **3–S**, respectively, indicating a late apoptosis state. None of the sulfur-based ligands or complexes induces necrotic cell death. All selenium-based compounds after 24 h of treatment displayed a significant decrease in the percentage of surviving cells. Moreover, a significant increase in late cellular apoptosis was observed. **HLSe^1**, **2–Se**, and **1–Se** exhibit similar elevation of late apoptotic cells at the level of ~20%. The strongest pro-apoptotic properties were exhibited by **HLSe^2** and **3–Se**, which was observed accordingly in 37.4 ± 3.4% and 41.8 ± 5.3% late apoptotic cells. As depicted in Figs. 7 and 48 h of treatment by **HLSe^1** and **HLSe^2** caused a 1.7-fold and 1.9-fold decrease of the percentage of apoptotic cells for the increase of necrotic fraction up to accordingly 15.8 ± 1.5% and 31.8 ± 4.3% of cells. Whereas compounds **1–Se**, **2–Se**, and **3–Se** increased a percentage of apoptotic cells, where the most conspicuous elevation was observed for **1–Se**, indicating a 2.1-fold increase in comparison to 24 h of treatment. It should be noted that the complexation of selenium-based ligands results in a decrease of necrotic cells without altering the pro-apoptotic properties of these compounds, except **1–Se**, which elicited twice the apoptosis before complexing. Additionally, it is worth emphasizing that in the case of cisplatin and etoposide, the percentage of apoptotic cells after 48 h of treatment (early + late) was only 16.8 ± 1.4% (cisplatin) and 15.3 ± 1.7% (etoposide). The obtained results of apoptosis are also confirmed by the microscopic imaging shown in Fig. 8. To visualization the structure of the cytoskeleton, cells were labeled with β-tubulin, a component of microtubules and with actin-binding protein cortactin, involved in signal transduction pathways and the cytoskeleton, enabling migration [26,27]. Treatment of T-47D cells with GI_{50} of compounds for 24 h showed evident morphological changes, including cell shrinkage, nuclear fragmentation, chromatin condensation, and finally formation of apoptotic bodies, characteristics of apoptotic cells. There were no apparent changes in the structure of the cytoskeleton after exposure to compounds. However, a significant decrease in cortactin fluorescence was noted in **2–Se** and **3–Se** compounds, indicating a 2.1-fold and 3.4-fold decrease in comparison to control (Fig. 9). This may suggest that the ability to form lamellipodia is disturbed, and thus the migration of the cells may be reduced, but indeed additional studies should be carried out in the future to confirm the anti-migratory properties of these compounds.

Apoptotic signaling pathways generally function through two major pathways – the death receptor-mediated (extrinsic) pathway and the mitochondria-mediated (intrinsic) pathway [28]. The extrinsic and intrinsic apoptosis pathways both involve caspases with specific cysteine protease activity, which trigger cell death by cleaving specific proteins in the cytoplasm and nucleus [29]. Since, caspase-3 and -7, together are a molecular key effector between these apoptotic pathways, the effect of compounds on activation of caspase-3/7 was tested by flow cytometry after treatment of T-47D cells with investigated compounds [30]. The results are shown in representative histograms and a bar chart in Fig. 10. For sulfur-based compounds and reference compounds (cisplatin, etoposide) the results were nearly identical to those observed when staining with Annexin-V-FITC/PI at the same time points: cells showed caspase fluorescence at a similar level as in the control. Selenium-based compounds strongly activated caspase-3/7 after 24 h of treatment and remained permanent for the next 24 h, except **HLSe^2**, which decreased caspase level by 19.1 ± 0.4%. A 48 h of treatment with compounds **2–Se** and **3–Se** most increased the expression of caspases 3/7, resulting in accordingly 10.7-fold and 13.0-fold elevation of caspase level in comparison to the vehicle, which is consistent with the results obtained in the Annexin-V-FITC/PI assay. Overall, these results point to the conclusion that selenium-based compounds led T-47D cells to apoptotic cell death associated with caspases.

Autophagy is an important mechanism for cell death regulation, by sequestering cytoplasmic proteins into the lytic component, which is associated with the formation of acidic vesicular organelles (AVOs). Thus, we investigated the effect of tested compounds on autophagy induction/repression by Acridine Orange (AO) staining. AO is a pH-sensitive lysotrophic fluorescence dye, with a green emission band when is co-localized with cytoplasm, but when is trapped within acidic vehicles, like lysosomes or Golgi Apparatus, forms aggregates that emit bright red fluorescence [31]. AO staining revealed that compounds **1–Se**, **HLSe^2**, **2–Se**, and **3–Se** significantly decrease red fluorescence (Figs. 11 and 12). Interestingly, in the case of **2–Se** and **3–Se**, the pronounced disappearance of the red fluorescence is noticeable, which indicates the potent alkalization of acid cell organelles. Alteration of extracellular pH of a tumor could be an effective target for cancer therapy because the cancer microenvironment plays an important role in the development of tumors, including response to therapy and chemoresistance [32,33]. During the late stage of autophagy,

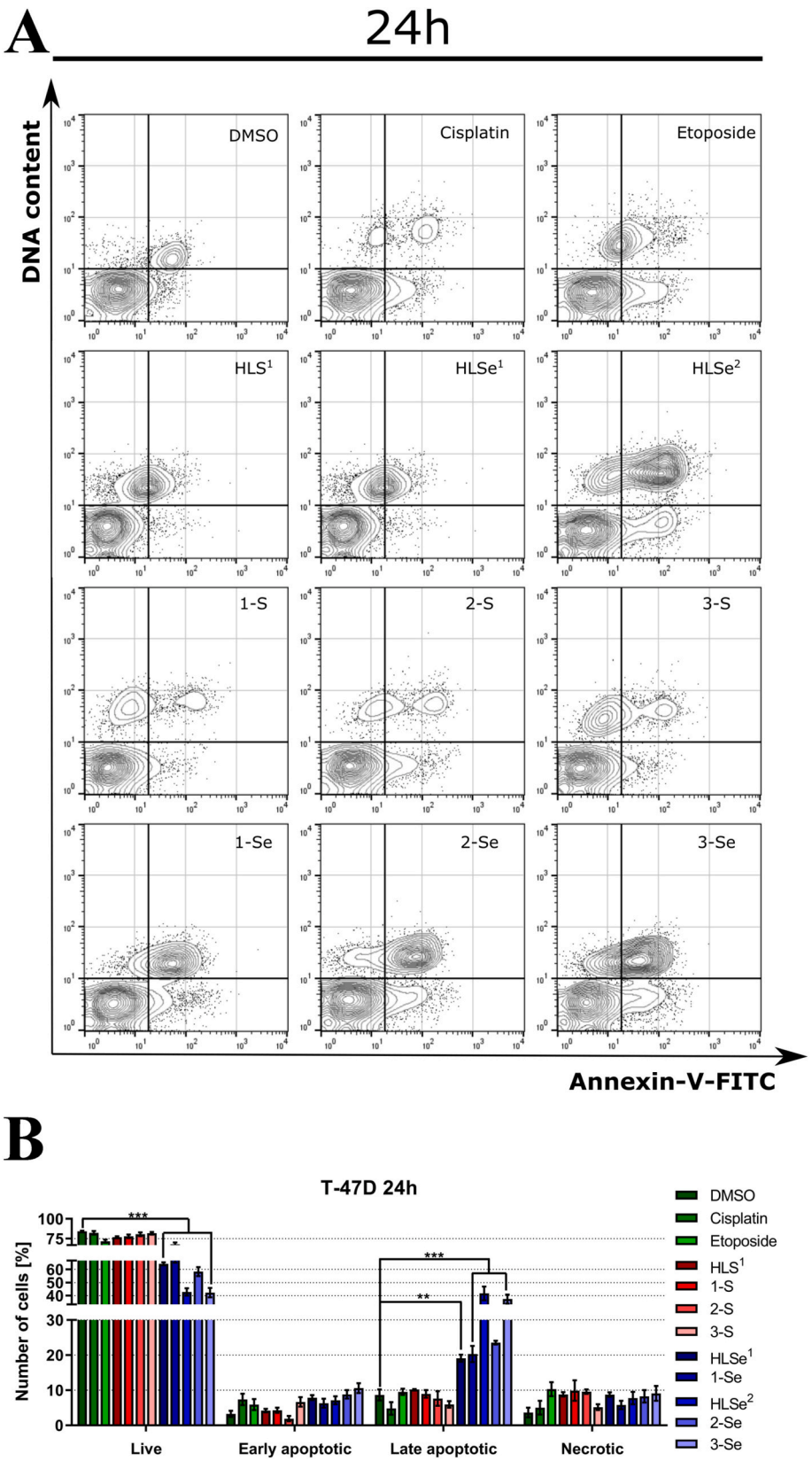

Fig. 6. Flow cytometry analyses of T-47D cells after 24 h. DMSO, etoposide, and cisplatin were used as reference compounds. (A) Representative dot-plots after labeling with Annexin-V-FITC/PI. (B) The quantitation of analysis is presented on a graph bar. Error bars represent the SEM of data obtained in n = 4 independent experiments. Statistical differences were analyzed with a two-way ANOVA test. ns > 0.05, *p < 0.01, **p < 0.001,***p < 0.0001 compared to DMSO.

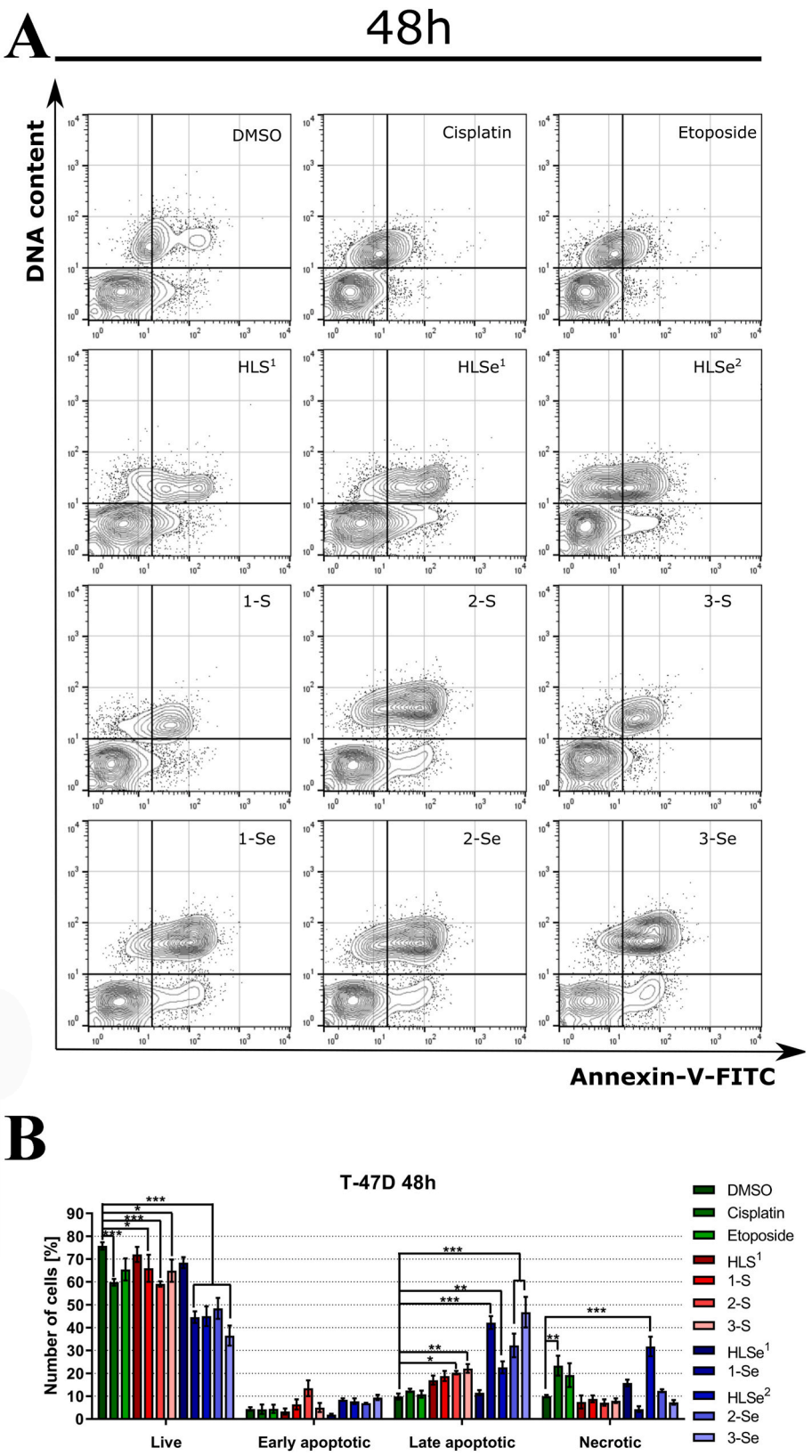

Fig. 7. Flow cytometry analyses of T-47D cells after 48 h of treatment. DMSO, etoposide, and cisplatin were used as reference compounds. (A) Representative dot-plots after labeling with Annexin-V-FITC/PI. (B) The quantitation of analysis is presented on a graph bar. Error bars represent the SEM of data obtained in n = 4 independent experiments. Statistical differences were analyzed with a two-way ANOVA test. ns > 0.05, *p < 0.01, **p < 0.001,***p < 0.0001 compared to DMSO.

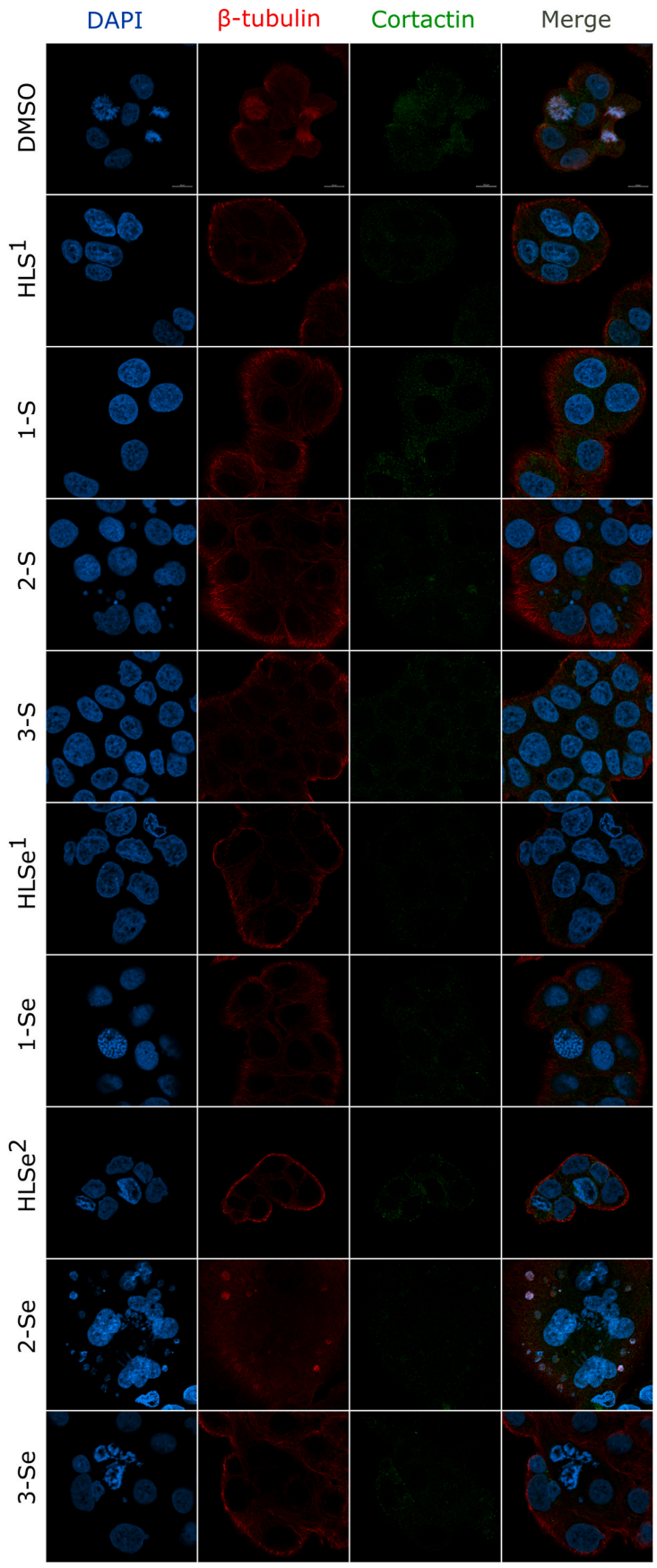

Fig. 8. Representative confocal images of T-47D cells morphology 24 h after treatment with tested compounds. The microtubule is depicted in red, cortactin in green, and the nucleus is stained DAPI (blue). Scale bars: 10 μm.

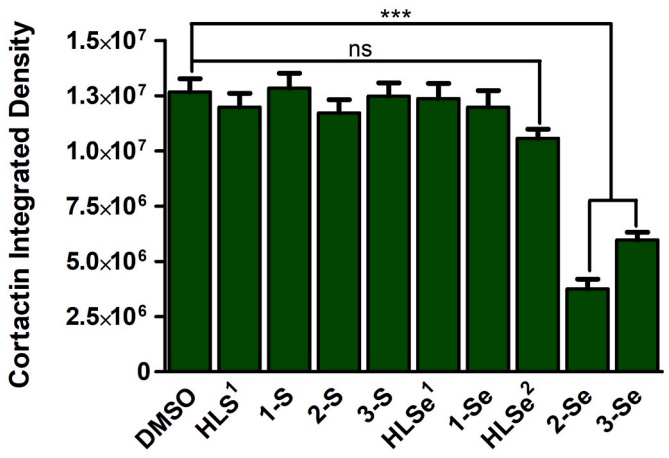

Fig. 9. Bar graph representation of the quantitation of the mean cortactin fluorescence intensity in control and compounds-treated T-47D cells. Error bars represent the SEM of data obtained in at least n = 15 randomly selected locations on the slide. Statistical differences were analyzed with a two-way ANOVA test. ns > 0.05, ***p < 0.0001 compared to DMSO.

autophagosomes maturate and fuse with lysosomes forming autolysosomes for degradation of cellular components [34]. To further confirm the influence of compounds on autophagy, double immune-staining with microtubule-associated protein (LC3B) and lysosomal-associated membrane protein 1 (LAMP-1) was performed after 24 h of treatment T-47D cells with tested compounds or chloroquine, as reference compound (Fig. 13). The co-localization of punctate LC3 and LAMP-1 was assayed using confocal microscopy and presented on a violin graph using Mander's overlap coefficient (Fig. S52, ESI). All tested ligands decreased a co-localization of punctate LC3 and LAMP-1, but mostly not significant (p value > 0.05), besides **HLS^1** (p value < 0.0001) and **HLSe^1** (p value < 0.01), and chloroquine (p value < 0.001). This observation can be associated with blocking the degradation of autolysosomes, and thereby inhibition of autophagy by these compounds. However, the complexation of these ligands results in the formation of autolysosomes, to the same extent as in control, despite the significant increase in pH of cells treated with these complexes. Thus, the determination of molecular machinery of intracellular pH dysregulation and the consequent effects in T-47D cells by these compounds should be the subject of further research.

2.2.5. DNA interactions

We investigated the effect of **HLS$^{1–3}$**, **HLSe$^{1–3}$** ligands and **1–3S**, **1–3Se** complexes on pBlueScript SK (−) plasmid in 5 mM Tris buffer (pH = 7.2) within 90 min of incubation/exposition in the range of concentrations (50–1000 μM). As it is shown in (lane 9) Fig. S53 (ESI) and Fig. 14, pBlueScript SK (−) plasmid DNA consists mainly of supercoiled circular (SC) form, while the presence of the other two forms has been also observed. Our results indicate that there is no nuclease activity or covalent binding of investigated ligands on plasmid DNA after 90 min of incubation (Fig. S53, ESI), while significant nuclease activity was detected for all Cd complexes with pyridine-based chalcogenazoles (Fig. 14). The strongest nuclease activity of all Cd complexes with pyridine-based chalcogenazoles was obtained at a concentration of 200 μM (lane 4). Interestingly, higher concentrations of Cd complexes exhibit lower nuclease activity. This might be due to formation of oligomeric structures of the complexes through stacking interactions of aromatic rings. Since we were able to detect nuclease activity even at the lowest tested concentrations of Cd complexes, we can assume that the possible mechanism of antiproliferative activity is their nuclease activity, which was not detected by any of the tested concentrations of the corresponding ligands (Fig. S53, ESI).

3. Conclusion

Cadmium complexes (**1–3Se**) with SHs ligands **HLSe$^{1–3}$** containing four heteroatoms (three nitrogen atoms and one selenium atom) were prepared. Characterization of **1–3Se** by a single-crystal XRD revealed that SHs ligands act as NNN tridentates. Two ligands coordinated to every Cd center are arranged in an octahedral geometry. Stability constants of all complexes, determined by spectrophotometric titrations, indicate their significant stability in solution, while **1–3Se** were more stable than their counterparts.

Investigation of anticancer activity of **HLS$^{1–3}$** and **HLSe$^{1–3}$** ligands and corresponding Cd complexes was conducted to evaluate the impact of substitution at ligands' periphery, chalcogen atom type, as well as complexation on the activity of the tested species. An antiproliferative activity study performed at six cancer cell lines revealed that all complexes are more active compared to 5-FU and cisplatin. The complexation of ligands with Cd resulted in a synergistic effect. This is the most obvious for **HLS^2**, which was non-active against all investigated cell lines. In addition, all six ligands were not active on WiDr cells. Generally, obtained GI_{50} values indicate that complexes **1–3S** are more active than their counterparts. On the other hand, GI_{50} values determined on healthy cell line indicate that both selenium-based ligands and complexes are less toxic in comparison to their sulfur-based counterparts. Acute toxicity studies indicated that the complexation marginally increased the acute toxicity of the tested compounds. However, it should be noted that the obtained LC_{50} values are significantly higher than the GI_{50} values. Overall, the complexation of compounds elevated antitumor activity with a slight increase in acute toxicity.

More detailed studies on the mechanism of tumor cell growth inhibition reveal that selenium-based compounds induce cell death in T-47D cells through apoptosis *via* caspase 3/7 activation. Additionally, the pro-apoptotic properties of these compounds are more pronounced after their complexation. It is worth noting that the pro-apoptotic effect of selenium-based compounds was stronger compared to etoposide and cisplatin, used as references. The mechanism of action of investigated sulfur-based compounds has not been identified in this work. Nevertheless, the high cytotoxic activity of these compounds is certainly worth additional research in the future in order to determine the exact molecular path that leads to cancer cell death. Nuclease activity of **1–3S** and **1–3Se,** detected by gel electrophoresis, may be the possible mechanism of anticancer action of investigated complexes. The same activity was not observed in the case of **HLS$^{1–3}$** and **HLSe$^{1–3}$**.

In summary, our results indicate the significant anticancer potency of Cd complexes with THs/SHs ligands. The results indicate the importance of chalcogen atom type and ligands peripheral substitution on activities studied herein. Taking into account the fact that Cd complexes with THs/SHs ligands induce favorable cell death in cancer cells, and despite the fact that these compounds also manifest significant activity against healthy cells, the current state of the development of delivery systems were a metal-based drug is delivered directly to tumor sites indicates their suitability for future studies.

4. Experimental selection

4.1. Materials and methods

4.1.1. General procedures

The chemicals which were used in the synthesis: 2-Pyridinecarboxaldehyde 99%, 2-Bromoacetophenone 98%, 2-Bromo-4′-methylacetophenone and 2-Bromo-4′-methoxyacetophenone 98% by Acros Organics, Thiosemicarbazide 99% by Alfa Aesar, Cadmium nitrate tetrahydrate 98% by Sigma Aldrich, Cadmium perchlorate hexahydrate by Fisher Scientific. All solvents (96% ethanol, methanol, dimethyl sulfoxide) were of reagent purity and used without further purification.

Elemental analyses (C, H, N, S) were performed by the standard micro methods using the ELEMENTAR Vario EL III CHNS/O analyzer.

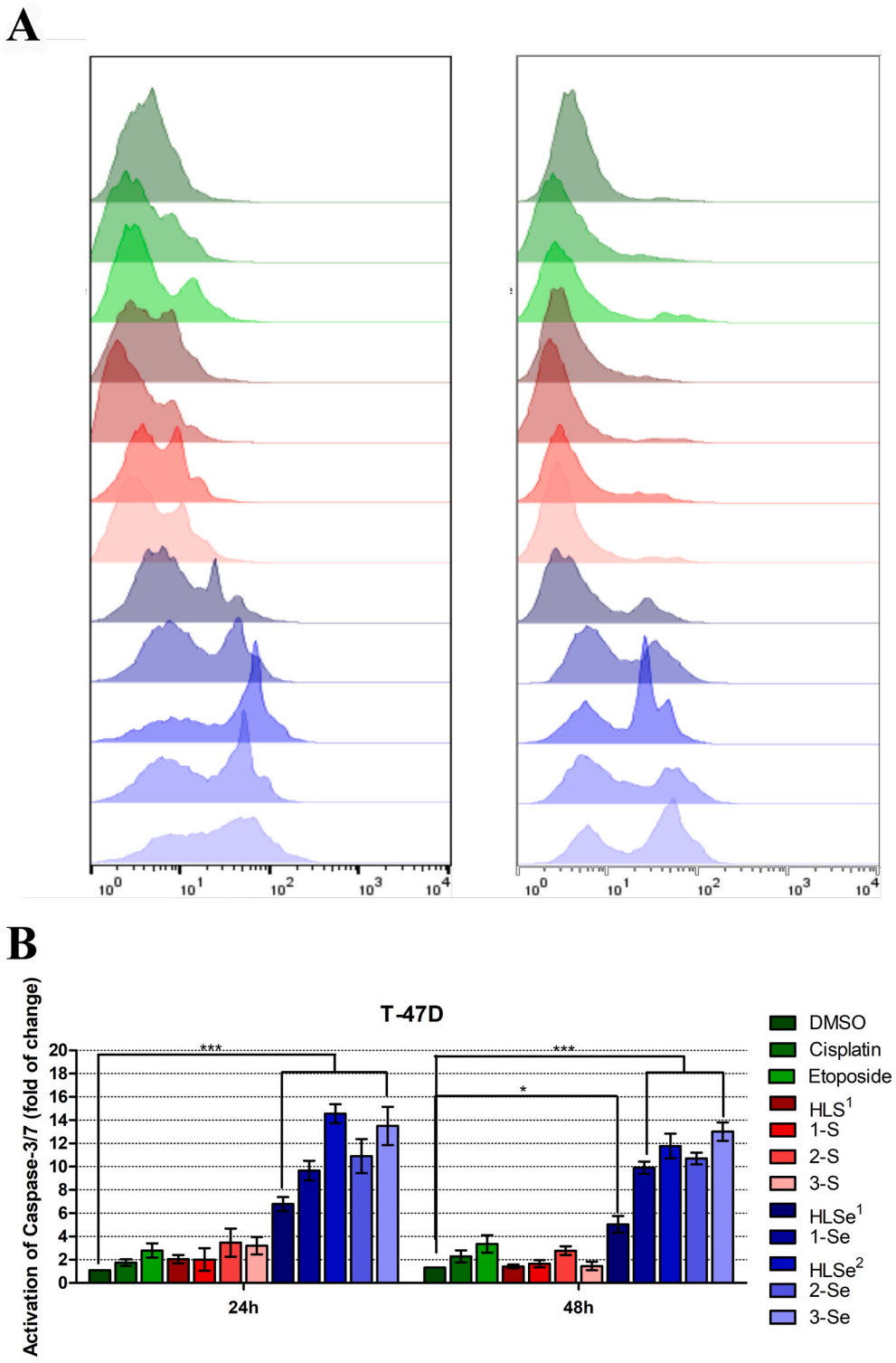

Fig. 10. Modulation of caspase-3/7 in T-47D cells after 24 h and 48 h treatment with compounds. DMSO, etoposide, and cisplatin were used as reference compounds. (A) Representative histograms after staining with CellEvent Caspase-3/7 Green Flow Cytometric Assay Kit measured by flow cytometry. (B) The quantitation of analysis is presented on a graph bar. Error bars represent the SEM of data obtained in n = 3 independent experiments. Statistical differences were analyzed with a two-way ANOVA test. ns > 0.05, *p < 0.01, ***p < 0.0001 compared to DMSO.

Infrared spectra (IR) were recorded with a Spectrum Two instrument (PerkinElmer) in the wavenumber range 4000−450 cm^{-1}, using the universal attenuated total reflection (UATR) technique. The method used was insensitive to sample thickness or shape due to the presence of the UATR hard crystal material. The apparatus was equipped with a diamond material with a measurable surface of about 4 mm^2, allowing good contact with samples. Abbreviations used in IR spectroscopy are w-weak; ms-medium strong; s-strong; vs-very strong. 1D and 2D nuclear magnetic resonance (NMR) spectra were recorded at 298 K in DMSO-d_6 with tetramethyl-silane (TMS) as an internal standard on a Bruker Avance III 500 spectrometer. Chemical shifts (δ) are given in ppm. Abbreviations used for NMR spectra: s-singlet; d-doublet; t-triplet, m-multiplet; dd-doublet of doublets; ddd-double-double doublet. Molar conductivity measurements were performed at ambient temperature (298 K) on a Crison Multimeter MM41 instrument.

All X-ray crystallography data collections were performed at room temperature on an Xcalibur Ruby Nova diffractometer with copper radiation (λ = 1.54183 Å). Data reduction and cell refinement were

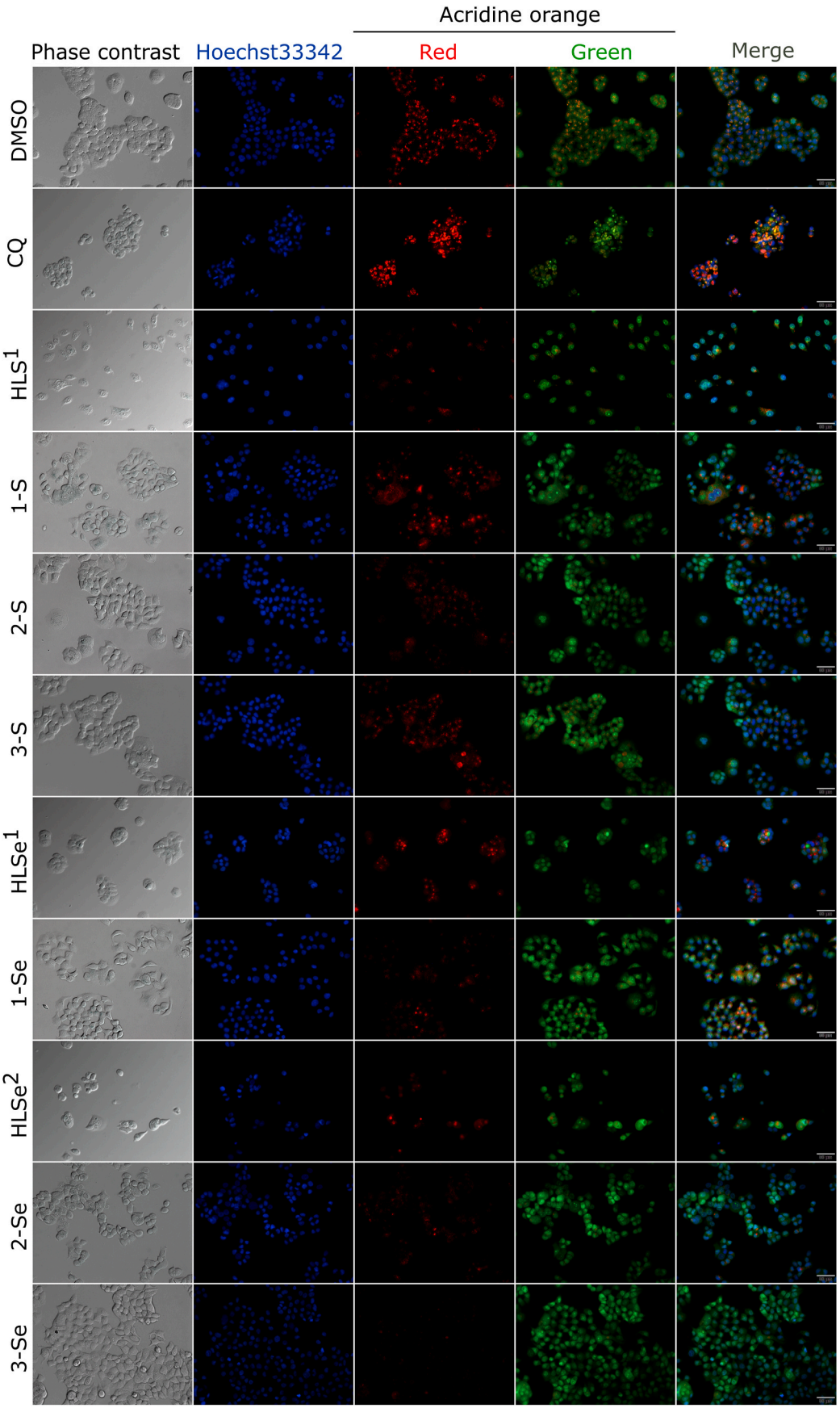

Fig. 11. Representative microscopic images of T-47D cells after 24 h of treatment with tested compounds after staining with Acridine orange and Hoechst 33342. Scale bar: 50 μm. DMSO and chloroquine (CQ) were used as reference compounds.

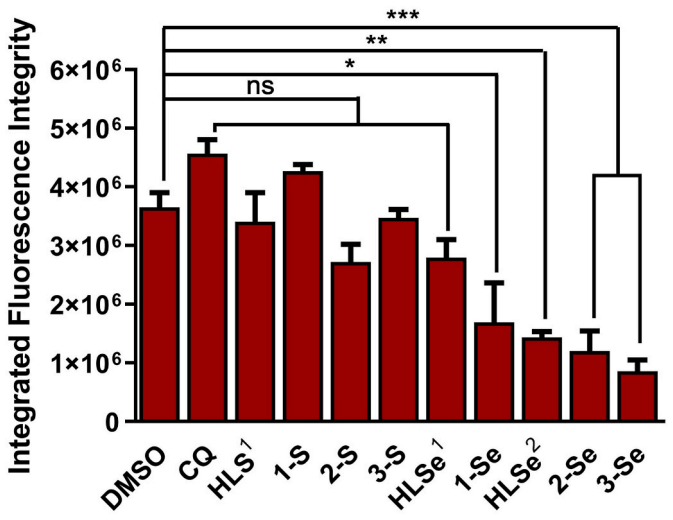

Fig. 12. Bar graph representation of the quantitation of the mean red fluorescence intensity in control and compounds-treated T-47D cells. Error bars represent the SEM of data obtained in at least n = 15 randomly selected locations on the slide. Statistical differences were analyzed with a two-way ANOVA test. ns > 0.05, *p < 0.01, **p < 0.001, ***p < 0.0001 compared to DMSO.

carried out using the CRYSALIS PRO software [35], and standard multi-scan absorption correction was applied. Structures were solved by direct methods with SIR2014 [36] and refined by a full-matrix least-squares refinement based on F^2, with SHELXL [37]. Molecular illustrations were prepared with MERCURY [38] included into the WinGX package [39]. Calculations of molecular geometries and crystal packing parameters were performed with PLATON [40]. Hydrogen atoms were either included in their geometrically calculated positions and refined according to the riding model, or, in some cases, located in the difference maps. CCDC 2077634–2077,639 contain the supplementary crystallographic data. These data can be obtained free of charge *via* http://www.ccdc.cam.ac.uk/conts/retrieving.html, or from the Cambridge Crystallographic Data Center, 12 Union Road, Cambridge CB2 1EZ, UK; fax:(+44) 1223-336-033; or e-mail: deposit@ccdc.cam.ac.uk.

Determination of the stability constants of the formed complexes was done by spectrophotometric titration at a constant concentration of the ligands. A UV–Vis Evolution 300 spectrophotometer was used to record electronic spectra in the 200–600 nm range with a spectral bandwidth of 1 nm. The samples were prepared in methanol directly before measurements. Cadmium perchlorate and cadmium nitrate were used as the source of Cd^{2+} ions. The spectrophotometric monitoring of complex formations was carried out on samples containing appropriate ligands with Cd^{2+} ions. During the experiments, the ligands' concentration was kept constant, which allowed the observation of spectral changes caused by the interaction of metal cation and ligands. A magnetic stirrer was placed in the measuring cuvette to continuously mix the titrant with the analyte. The spectrophotometric titration procedure was performed using the CerkoLab System automatic titrator equipped with a 1 mL Hamilton syringe. A single titration step was 8.74 μl. During each titration cycle, the constants temperature (25 °C) was kept by a jacketed titration cell connected to Lauda circulating thermostatic system (temp. accuracy ±0.10 °C). Measurement data was processed in the OriginLab program. The gradual and cumulative stability constants of complex compounds were determined using the EQUID computational program by A. Liwo and J. Kostrowicki [41,42].

4.1.2. Antiproliferative activity

For the antiproliferative tests, we applied our implementation of the National Cancer Institute (NCI) screening protocol [43]. We used as a model of human solid tumor cells the following cell lines: A549 (non-small cell lung), HBL-100 (breast), HeLa (cervix), SW1573 (non-small

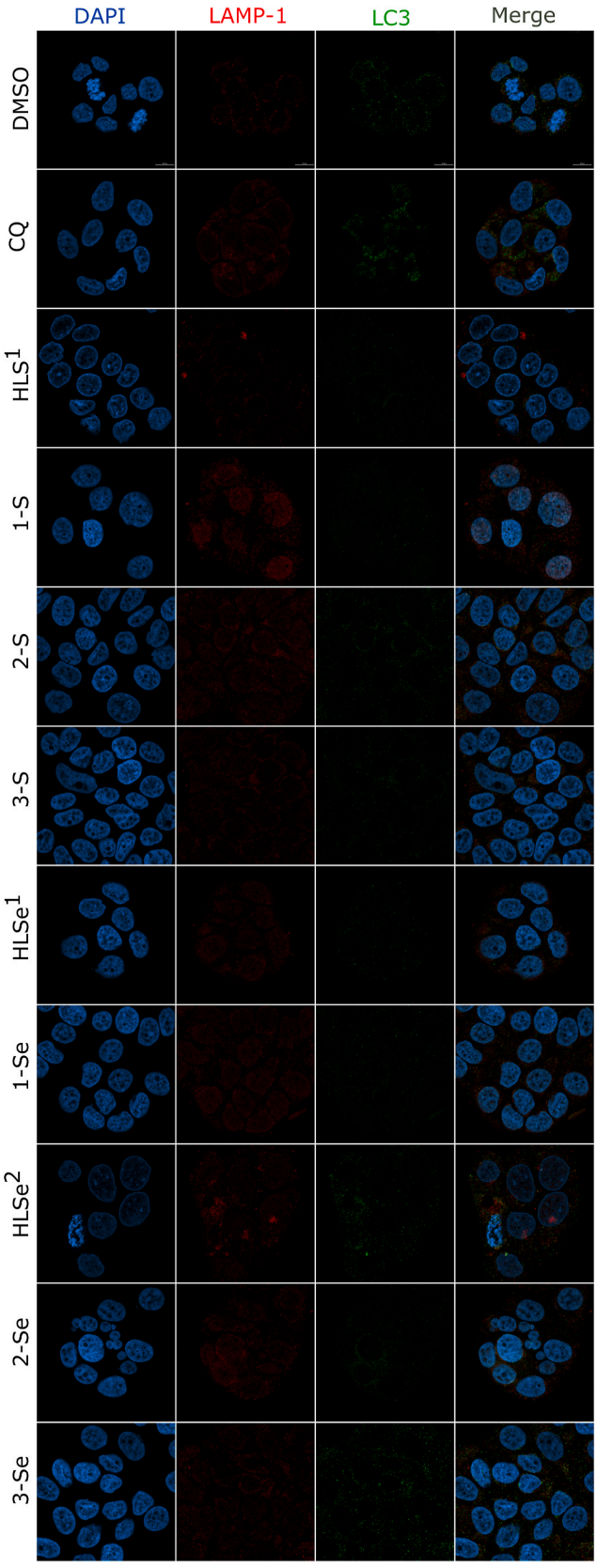

Fig. 13. Representative confocal images of T-47D cells after 24 h of treatment with tested compounds. LC3B is depicted in green, LAMP-1 in red, and the nucleus is stained DAPI (blue). Scale bars: 10 μm.

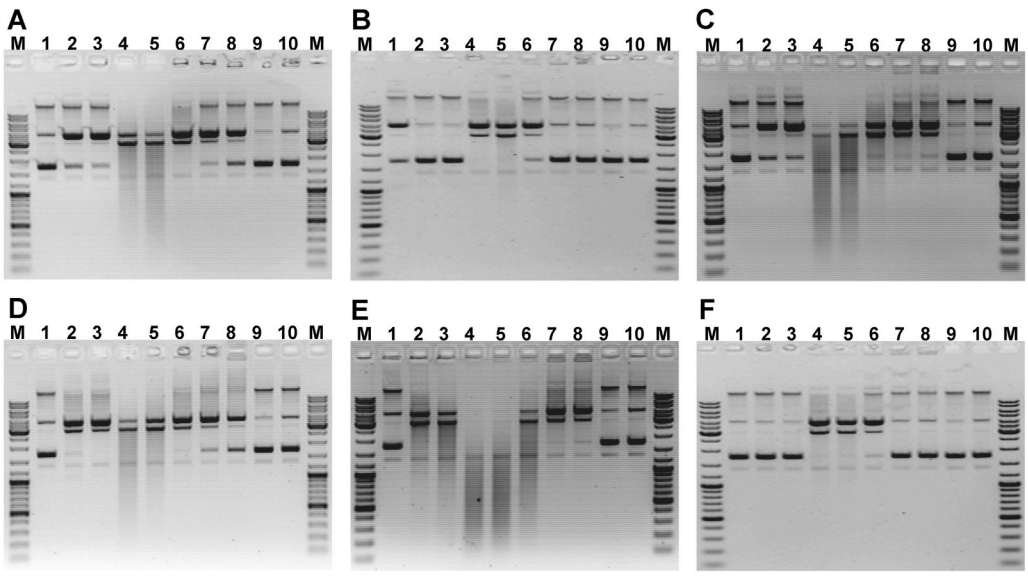

Fig. 14. Interaction result on 1% agarose electrophoresis of pBlueScript SK (−) plasmid DNA with tested thiazole-based complexes: **1–S** (A), **2–S** (B), **3–S** (C), and selenazole-based complexes: **1–Se** (D), **2–Se** (E) and **3–Se** (F) after 90 min of incubation at 37 °C. Lane M – Gene Ruler DNA Ladder Mix 0.1–10 kb (Thermo Fisher Scientific), lane 1, 2, 3, 4, 5, 6, 7 and 8 – plasmid pBlueScript SK (−) DNA with 0, 50 μM, 100 μM, 200 μM, 300 μM, 500 μM, 750 μM and 1000 μM of the corresponding complex, respectively; lane 9 – control plasmid pBlueScript SK (−) DNA; lane 10 – control plasmid pBlueScript SK (−) DNA + 3 μM of DMSO.

cell lung), T-47D (breast), and WiDr (colon). The antiproliferative activity was tested also on the non-cancerous HEK293 cell line. Cell seeding densities were 2500 (A549, HBL-100, HeLa, SW1573 and HEK293) or 5000 (T-47D and WiDr) cells/well. Cells were treated according to the protocol described earlier [43]. Tested compounds were dissolved in DMSO at an initial concentration of 40 mM. DMSO was used as negative control (0.25% v/v). The results were expressed as GI_{50}, i.e. the dose that causes 50% growth inhibition after 48 h of exposure.

4.1.3. *Artemia salina cytotoxicity test*

A teaspoon of lyophilized eggs of the brine shrimp *Artemia salina* was added to 1 l of the artificial seawater and the air was passed through the suspension thermostated at 301 K, under illumination for 24 h. The tested substances were dissolved in DMSO, while cisplatin was dissolved in phosphate-buffered saline (pH 7.4). In a glass vial, filled with 1 mL of artificial seawater containing 10–20 freshly hatched nauplii, finally solutions of all tested compounds to the appropriate concentrations were added. For each concentration, three determinations were performed. The vials were left at 301 K under illumination for 24 h, and afterward, live and dead nauplii were counted. LC_{50} was defined as the concentration of a drug that causes the death of 50% nauplii. Potassium dichromate served as a positive control and DMSO was inactive under applied conditions.

4.1.4. *Apoptosis and caspase-3/7 assay*

Briefly, T-47D cells were seeded in Petri dishes to attach overnight. In total, 2×10^5 cells were treated with GI_{50} concentrations of investigated compounds or etoposide and cisplatin for 24 and 48 h. Cells were stained with fluorescein isothiocyanate (FITC) - Annexin V, Alexa Fluor™ 488 conjugate (Thermo Fisher, #A13201) for apoptosis assay and with CellEvent™ Caspase-3/7 Green Flow Cytometry Assay Kit (Thermo Fisher, #C10427) for caspase-3/7 activation test according to the manufacturer's protocols. Thereafter, cells were stained with Propidium Iodide (PI) (Sigma Aldrich) and analyzed by flow cytometry using a Guava easyCyte 8 cell sorter (Merck Millipore) and FlowJo v10 software.

4.1.5. *Cell cycle distribution analysis*

The effect of ligands and complexes on T-47D cell cycle distribution was determined by flow cytometric analysis. Etoposide (Sigma-Aldrich) was used as a reference compound. Cells were exposed to compounds in their GI_{50} concentrations for 24 and 48 h and then harvested, fixed with ice-cold 75% ethanol, and stored overnight at −20 °C. Cells were then rehydrated with Phosphate-buffered saline (PBS), stained with 20 μg/μl PI (Sigma-Aldrich) and 50 μg/μL RNaseA (Thermo Fisher), and analyzed by flow cytometry using a Guava easyCyte 8 cell sorter (Merck Millipore) and FlowJo v10 software.

4.1.6. *Live-cell imaging*

For the detection of basification of acidic organelles T-47D cell line was treated with ligands and complexes in their GI50 concentrations for 24 h. 1% DMSO (Merck) and 70 μM chloroquine (Sigma-Aldrich) were used as references. After treatment, Acridine orange (Sigma-Aldrich) and Hoechst 33,342 (Thermo-Fisher) were added at 1 μg/mL to the culture media 30 min before image acquisition. Subsequently, cells were washed twice with warm Hank's Balanced Salt Solution (Thermo-Fisher) and imaged by inverted fluorescence microscope BX60 (Olympus) using x20 XC50 objective.

4.1.7. *Immunofluorescence*

T-47D breast cells were treated with ligands and complexes in their GI50 concentrations for 24 h, fixed with 4% paraformaldehyde for 15 min, permeabilized with 0.2% Triton-X 100 for 10 min, and then blocked with 3% BSA (Sigma-Aldrich) in PBS-T (PBS with 0.1% Triton X-100) for 1 h at RT. β-Tubulin (Sigma-Aldrich, #T8328), Cortactin (H222) (Cell Signaling, #3503), LC3B (Cell Signaling, #2775), and LAMP1 (D4O1S) (Cell Signaling, #15665) antibodies were added at 1 : 250 for 1 h in a humidified chamber at 37 °C, followed by Alexa-Fluor-594-conjugated anti-rabbit IgG (Santa Cruz Biotechnology, #sc-516,250) or Alexa-Fluor-488-conjugated anti-mouse IgG (Invitrogen, #SA5-10166) at 1:1000 for 1 h in a humidified chamber at 37 °C. After labeling, nuclei were stained with 1 μg/mL DAPI (Sigma-Aldrich) for 10 min. Images were acquired with an LSM 800 inverted laser-scanning confocal microscope (Carl Zeiss), airyscan detector for higher resolution confocal scanning using a × 63 1.4 NA Plan Apochromat objective (Carl Zeiss). Correlations of overlapping pixel intensities were calculated using thresholded Mander's (MCC) colocalization coefficient using the JACoP plugin for Image J as previously described [44].

4.1.8. *Gel electrophoresis study of interactions with plasmid DNA*

The interactions of complexes with plasmid DNA were investigated by agarose gel electrophoresis. pBlueScript SK (−) plasmid (0.01 M) in 5 mM Tris buffer (pH = 7.2) was treated with complexes at 37 °C. The samples were incubated for 90 and 120 min, and then a loading buffer was added to stop the reaction. The samples were then examined by electrophoresis at 6 V cm^{-1} on 1% agarose gel using Tris–boric

acid–EDTA buffer. After electrophoresis, the bands were visualized using UV light and photographed. The cleavage reaction was initiated by the addition of the complex and quenched with 2 μL of the loading buffer.

4.2. Chemistry

4.2.1. Preparation of the ligands

Ligands **HLS$^{1-3}$** and **HLSe$^{1-3}$** were synthesized according to the reported literature method [19]. Ligands were prepared in two steps by condensation reaction between 2-pyridinecarboxaldehyde with thiosemicarbazide or selenosemicarbazide. The resulting thio/-selenosemicarbazon is further condensed with the corresponding α-halocarbonyl compounds by the Hantzsch reaction. Elemental analysis, IR, and NMR spectra of ligands are in agreement with the previously published results [19].

4.2.2. General procedure for the synthesis of Cd complexes

Into suspension of the corresponding ligand (0.18 mmol for **1-S**; 0.16 mmol for **2-S**; 0.17 mmol for **3-S**; 0.15 mmol for **1-Se** and **3-Se**; 0.14 mmol for **2-Se**; 1.0 equiv.) in MeOH (10 mL), a solution of Cd(II) salt in MeOH (10 mL) was added (0.5 equiv. of $Cd(ClO_4)_2{\cdot}6H_2O$ for **1-S**, **3-S**, **1-Se** and **3-Se** or 0.5 equiv. of $Cd(NO_3)_2{\cdot}4H_2O$ for **2-S** and **2-Se**). The reaction mixture was refluxed for 1 h. The single crystals of the complexes, obtained from the mother liquor, were filtered off and washed with cold MeOH.

Declaration of competing interest

The authors declare that they have no known competing financial interests or personal relationships that could have appeared to influence the work reported in this paper.

Acknowledgments

The authors acknowledge the financial support of the Ministry of Education, Science and Technological Development of the Republic of Serbia (Contract No's. 451-03-68/2022-14/200168 and 451-03-68/2022-14/200116). A.P. and J.M.P. thank the Spanish Government (PGC2018-094503-B-C22, MCIU/AEI/FEDER, UE) and the Canary Islands Government (ProID2020010101, ACIISI/FEDER, UE) for financial support. A.P. thanks the EU Social Fund (FSE) and the Canary Islands ACIISI for a predoctoral grant TESIS2020010055.

Appendix A. Supplementary data

Supplementary data to this article can be found online at https://doi.org/10.1016/j.ejmech.2022.114449.

References

[1] D.S. Wishart, Y.D. Feunang, A.C. Guo, E.J. Lo, A. Marcu, J.R. Grant, T. Sajed, D. Johnson, C. Li, Z. Sayeeda, N. Assempour, I. Iynkkaran, Y. Liu, A. Maciejewski, N. Gale, A. Wilson, L. Chin, R. Cummings, D. Le, A. Pon, C. Knox, M. Wilson, DrugBank 5.0: a major update to the DrugBank database for 2018, Nucleic Acids Res. 46 (2018) D1074–D1082, https://doi.org/10.1093/nar/gkx1037.

[2] A. Valente, A. Podolski-Renić, I. Poetsch, N. Filipović, Ó. López, I. Turel, P. Heffeter, Metal- and metalloid-based compounds to target and reverse cancer multidrug resistance, Drug Resist. Updates 58 (2021), 100778, https://doi.org/10.1016/j.drup.2021.100778.

[3] E.J. Anthony, E.M. Bolitho, H.E. Bridgewater, O.W.L. Carter, J.M. Donnelly, C. Imberti, E.C. Lant, F. Lermyte, R.J. Needham, M. Palau, P.J. Sadler, H. Shi, F. X. Wang, W.Y. Zhang, Z. Zhang, Metallodrugs are unique: opportunities and challenges of discovery and development, Chem. Sci. 11 (2020) 12888–12917, https://doi.org/10.1039/d0sc04082g.

[4] A. Frei, Metal complexes, an untapped source of antibiotic potential? Antibiotics 9 (2020) 90, https://doi.org/10.3390/antibiotics9020090.

[5] S. Alcaro, M.L. Bolognesi, A.T. García-Sosa, S. Rapposelli, Editorial: multi-target-directed ligands (MTDL) as challenging research tools in drug discovery: from design to pharmacological evaluation, Front. Chem. 7 (2019) 1–2, https://doi.org/10.3389/fchem.2019.00071.

[6] Y. Zhao, Y. Yang, F. Xu, W. Zheng, Q. Luo, Y. Zhang, F. Jia, F. Wang, Pharmacophore Conjugation Strategy for Multi-Targeting Metal-Based Anticancer Complexes, first ed., Elsevier Inc., 2020 https://doi.org/10.1016/bs.adioch.2019.10.002.

[7] Y. Gou, G.J. Huang, J. Li, F. Yang, H. Liang, Versatile delivery systems for non-platinum metal-based anticancer therapeutic agents, Coord. Chem. Rev. 441 (2021), 213975, https://doi.org/10.1016/j.ccr.2021.213975.

[8] S.K. Bjelogrlić, T.R. Todorović, M. Kojić, M. Senćanski, M. Nikolić, A. Višnjevac, J. Araškov, M. Miljković, C.D. Muller, N.R. Filipović, Pd(II) complexes with N-heteroaromatic hydrazone ligands: anticancer activity, in silico and experimental target identification, J. Inorg. Biochem. 199 (2019), 110758, https://doi.org/10.1016/J.JINORGBIO.2019.110758.

[9] International Agency for Research on Cancer, Agents Classif. by IARC Monogr. Vol. 1–129. (n.d.).

[10] M. Schmid, S. Zimmermann, H.F. Krug, B. Sures, Influence of platinum, palladium and rhodium as compared with cadmium, nickel and chromium on cell viability and oxidative stress in human bronchial epithelial cells, Environ. Int. 33 (2007) 385–390, https://doi.org/10.1016/j.envint.2006.12.003.

[11] K.S. Egorova, V.P. Ananikov, Toxicity of metal compounds: knowledge and myths, Organometallics 36 (2017) 4071–4090, https://doi.org/10.1021/acs.organomet.7b00605.

[12] Z. Zhang, C. Bi, D. Buac, Y. Fan, X. Zhang, J. Zuo, P. Zhang, N. Zhang, L. Dong, Q. P. Dou, Organic cadmium complexes as proteasome inhibitors and apoptosis inducers in human breast cancer cells, J. Inorg. Biochem. 123 (2013) 1–10, https://doi.org/10.1016/j.jinorgbio.2013.02.004.

[13] S. Bjelogrlić, T.R. Todorović, I. Cvijetić, M.V. Rodić, M. Vujčić, S. Marković, J. Araškov, B. Janović, F. Emhemmed, C.D. Muller, N.R. Filipović, A novel binuclear hydrazone-based Cd(II) complex is a strong pro-apoptotic inducer with significant activity against 2D and 3D pancreatic cancer stem cells, J. Inorg. Biochem. 190 (2019) 45–66, https://doi.org/10.1016/J.JINORGBIO.2018.10.002.

[14] J.B. Araškov, M. Nikolić, S. Armaković, S. Armaković, M. Rodić, A. Višnjevac, J. M. Padrón, T.R. Todorović, N.R. Filipović, Structural, antioxidant, antiproliferative and in−silico study of pyridine-based hydrazonyl−selenazoles and their sulphur isosteres, J. Mol. Struct. 1240 (2021), https://doi.org/10.1016/j.molstruc.2021.130512.

[15] C.R. Groom, I.J. Bruno, M.P. Lightfoot, S.C. Ward, The Cambridge structural database, Acta Crystallogr. Sect. B Struct. Sci. Cryst. Eng. Mater. 72 (2016) 171–179, https://doi.org/10.1107/S2052520616003954.

[16] S. Rajabi, A. Ramazani, M. Hamidi, T. Naji, Artemia salina as a model organism in toxicity assessment of nanoparticles, DARU, J. Pharm. Sci. 23 (2015), https://doi.org/10.1186/s40199-015-0105-x.

[17] K.B. Horwitz, M.B. Mockus, B.A. Lessey, Variant T47D human breast cancer cells with high progesterone-receptor levels despite estrogen and antiestrogen resistance, Cell 28 (1982) 633–642, https://doi.org/10.1016/0092-8674(82)90218-5.

[18] K.C. Agrawal, B.A. Booth, R.L. Michaud, E.C. Moore, A.C. Sartorelli, Comparative studies of antineoplastic activity of 5-hydroxy-2-formylpyridine thiosemicarbazone and its seleno-semicarbazone, guanylhydrazone and semicarbazone analogs, Biochem. Pharmacol. 23 (1974) 2421–2429, https://doi.org/10.1016/0006-2952(74)90233-0.

[19] N.R. Filipović, H. Elshaflu, S. Grubišić, L.S. Jovanović, M. Rodić, I. Novaković, A. Malešević, I.S. Djordjević, H. Li, N. Šojić, A. Marinković, T.R. Todorović, Co(III) complexes of (1,3-selenazol-2-yl)hydrazones and their sulphur analogues, Dalton Trans. 46 (2017) 2910–2924, https://doi.org/10.1039/C6DT04785H.

[20] O.O. Ogbole, P.A. Segun, A.J. Adeniji, In vitro cytotoxic activity of medicinal plants from Nigeria ethnomedicine on Rhabdomyosarcoma cancer cell line and HPLC analysis of active extracts, BMC Compl. Alternative Med. 17 (2017) 1–11, https://doi.org/10.1186/s12906-017-2005-8.

[21] A. Lagarto Parra, R. Silva Yhebra, I. Guerra Sardiñas, L. Iglesias Buela, Comparative study of the assay of Artemia salina L. and the estimate of the medium lethal dose (LD50 value) in mice, to determine oral acute toxicity of plant extracts, Phytomedicine 8 (2001) 395–400, https://doi.org/10.1078/0944-7113-00044.

[22] J. Chu, Y. Zhu, Y. Liu, L. Sun, X. Lv, Y. Wu, P. Hu, F. Su, C. Gong, E. Song, B. Liu, Q. Liu, E2F7 overexpression leads to tamoxifen resistance in breast cancer cells by competing with E2F1 at miR-15a/16 promoter, Oncotarget 6 (2015) 31944–31957, https://doi.org/10.18632/oncotarget.5128.

[23] X. Liu, W. Yang, Z. Guan, W. Yu, B. Fan, N. Xu, D.J. Liao, There are only four basic modes of cell death, although there are many ad-hoc variants adapted to different situations, Cell Biosci. 8 (2018) 1–12, https://doi.org/10.1186/s13578-018-0206-6.

[24] G.Y.G. Zhang, V. Gurtu, S.R. Kain, Early detection of apoptosis using a fluorescent conjugate of annexin V, Biotechniques 23 (1997) 525–531.

[25] C. Riccardi, I. Nicoletti, Analysis of apoptosis by propidium iodide staining and flow cytometry, Nat. Protoc. 1 (2006) 1458–1461, https://doi.org/10.1038/nprot.2006.238.

[26] G.M.A.E. Nogales, Tubulin and Microtubule Structure: Mechanistic Insights into Dynamic Instability and its Biological Relevance, Reference Module in Life Sciences, Elsevier, 2017.

[27] E.R.A. Shvetsov, E. Berkane, D. Chereau, R. Dominguez, The actin-binding domain of cortactin is dynamic and unstructured and affects lateral and longitudinal contacts in F-actin, Cell Motil Cytoskeleton 66 (2009) 90–98.

[28] G. Xu, Y. Shi, Apoptosis signaling pathways and lymphocyte homeostasis, Cell Res. 17 (2007) 759–771, https://doi.org/10.1038/cr.2007.52.

[29] H.A. Harrington, K.L. Ho, S. Ghosh, K. Tung, Construction and analysis of a modular model of caspase activation in apoptosis, Theor. Biol. Med. Model. 5 (2008) 1–15, https://doi.org/10.1186/1742-4682-5-26.
[30] M. Brentnall, L. Rodriguez-Menocal, R.L. De Guevara, E. Cepero, L.H. Boise, Caspase-9, caspase-3 and caspase-7 have distinct roles during intrinsic apoptosis, BMC Cell Biol. 14 (2013) 1, https://doi.org/10.1186/1471-2121-14-32.
[31] R.K.A.S. Murugan, Methods for studying autophagy within the tumor microenvironment, Adv. Exp. Med. Biol. 899 (2016) 145–166.
[32] G. Hao, Z.P. Xu, L. Li, Manipulating extracellular tumour pH: an effective target for cancer therapy, RSC Adv. 8 (2018) 22182–22192, https://doi.org/10.1039/c8ra02095g.
[33] C. Ward, J. Meehan, M.E. Gray, A.F. Murray, D.J. Argyle, I.H. Kunkler, S. P. Langdon, The impact of tumour pH on cancer progression: strategies for clinical intervention, Explor. Target. Anti-Tumor Ther. 1 (2020) 71–100, https://doi.org/10.37349/etat.2020.00005.
[34] D. Glick, S. Barth, K.F. Macleod, Autophagy: cellular and molecular mechanisms, J. Pathol. 221 (2010) 3–12, https://doi.org/10.1002/path.2697.
[35] CrysAlis PRO. Agilent, U.K. Yarnton, Agilent Technologies, 2010.
[36] M.C. Burla, R. Caliandro, B. Carrozzini, G.L. Cascarano, C. Cuocci, C. Giacovazzo, M. Mallamo, A. Mazzone, G. Polidori, Crystal structure determination and refinement *via* SIR2014, J. Appl. Crystallogr. 48 (2015) 306–309, https://doi.org/10.1107/S1600576715001132.
[37] G.M. Sheldrick, Crystal structure refinement with SHELXL, Acta Crystallogr. Sect. C Struct. Chem. C71 (2015) 3–8, https://doi.org/10.1107/S2053229614024218.
[38] C.F. Macrae, I.J. Bruno, J.A. Chisholm, P.R. Edgington, P. McCabe, E. Pidcock, L. Rodriguez-Monge, R. Taylor, J. van de Streek, P.A. Wood, Mercury CSD 2.0 – new features for the visualization and investigation of crystal structures, J. Appl. Crystallogr. 41 (2008) 466–470, https://doi.org/10.1107/S0021889807067908.
[39] L.J. Farrugia, WinGX suite for small-molecule single-crystal crystallography, J. Appl. Crystallogr. 32 (1999) 837–838, https://doi.org/10.1107/S0021889899006020.
[40] A.L. Spek, Structure validation in chemical crystallography, Acta Crystallogr. Sect. D Biol. Crystallogr. 65 (2009) 148–155, https://doi.org/10.1107/S090744490804362X.
[41] J. Kostrowicki, A. Liwo, Determination of equilibrium parameters by minimization of an extended sum of squares, Talanta 37 (1990) 645–650, https://doi.org/10.1016/0039-9140(90)80211-W.
[42] J. Kostrowicki, A. Liwo, A general method for the determination of the stoichiometry of unknown species in multicomponent systems from physicochemical measurements, Comput. Chem. 11 (1987) 195–210, https://doi.org/10.1016/0097-8485(87)80018-9.
[43] H. Elshaflu, T.R. Todorović, M. Nikolić, A. Lolić, A. Višnjevac, S. Hagenow, J. M. Padrón, A.T. García-Sosa, I.S. Djordjević, S. Grubišić, H. Stark, N.R. Filipović, Selenazolyl-hydrazones as novel selective MAO inhibitors with antiproliferative and antioxidant activities: experimental and in-silico studies, Front. Chem. 6 (2018) 247, https://doi.org/10.3389/fchem.2018.00247.
[44] S. Bolte, F.P. Cordelières, A guided tour into subcellular colocalization analysis in light microscopy, J. Microsc. 224 (2006) 213–232, https://doi.org/10.1111/j.1365-2818.2006.01706.x.